Carbon 232 (2025) 119820

Contents lists available at ScienceDirect

Carbon

journal homepage: www.elsevier.com/locate/carbon

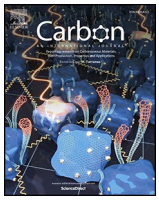

Electroactive covalent linkers for enhancing conducting polymer adhesion, charge transfer, and biological integration of PEDOT-coated carbon microfibers

Myriam Barrejón [a,b,*], Hugo Vara [a], Alexandra Alves-Sampaio [a], Helena Uceta [b], Jorge E. Collazos-Castro [a,**]

[a] Neural Repair and Biomaterials Laboratory, Hospital Nacional de Parapléjicos (SESCAM), Finca La Peraleda S-N, 45071, Toledo, Spain
[b] Instituto de Nanociencia, Nanotecnología y Materiales Moleculares, Universidad de Castilla-La Mancha, Avda. Carlos III, S/N, 45071, Toledo, Spain

ARTICLE INFO

Keywords:
Microfiber
Carbon
Conducting polymer
PEDOT
Covalent
Azidirine
Neural

ABSTRACT

Poly(3,4-ethylenedioxythiophene) (PEDOT)-coated carbon microfibers (PCMFs) are a key technology for developing advanced neuroprosthetic electrodes and electroactive tissue scaffolds. However, for their successful application in human therapeutics, PEDOT adhesion to the carbon substrate must be enhanced without compromising electric charge transfer. Here, electrically functional linkers are synthesized to modify the surface at the nanoscale, facilitating the covalent bonding of EDOT to carbon. The properties of the resulting microfibers are compared before and after PEDOT polymerization. PCMFs deterioration is studied by applying controlled mechanical stress *in vitro* or by implanting them in the rodent spinal cord *in vivo*. Amino phenyl-EDOT derivatives allow for efficient covalent carbon surface functionalization and PEDOT electropolymerization but substantially reduce charge transfer as assessed by chronopotentiometry, electrochemical impedance spectroscopy, and cyclic voltammetry. Nevertheless, the azido-EDOT (EDOT-Ph-N_3) derivative is similarly effective for carbon surface modification, enabling PEDOT polymerization to develop a nanostructured CMF surface based on robust covalent bonds, and enhancing both electric charge transfer and PEDOT adhesion to the carbon substrate. This makes PCMFs more resistant to polymer delamination when assessed *in vitro* or when implanted into the neural tissue. Azido-EDOT modified PCMFs also show excellent biological integration within the spinal cord, causing negligible tissue damage and cell reactivity. Overall, azido-EDOT provides a superior electroconducting linker for anchoring PEDOT and optimizes the electrical, mechanical, and biological performance of PCMFs.

1. Introduction

Electrodes coated with the conducting polymer poly(3,4-ethylenedioxythiophene) (PEDOT) result in composite materials with remarkable electrochemical properties, low electrochemical impedance, and substantially enhanced charge injection capacity [1–4], thus providing a powerful technology that may effectively face challenging medical applications demanding high-quality sensing or stimulation of bioelectrical activity. For instance, carbon microfibers coated with PEDOT doped with poly[(4-styrenesulfonic acid)-co-(maleic acid)] (PEDOT:PSS-*co*-MA) (PCMFs) allow for ultrasensitive recording of neuronal activity [5] and can be advantageously used for electrical micro-stimulation of the neural tissue [6]. Because of their small diameter (usually below 10 μm) and suitability for modification with biomolecules [7,8], PCMFs cause negligible tissue damage and show superior integration when implanted in the uninjured central nervous system [9]. These features make PCMFs also useful for the fabrication of implantable electroactive scaffolds aimed at promoting guided cell migration and axonal regeneration across spinal cord lesions [10]. Nevertheless, neurological applications of PCMFs are still hampered by the insufficient mechanical stability of the conducting polymer, which cracks and delaminates from the carbon surface when surgically handled for implantation or when chronically submitted to electrical stimulation in physiological electrolytes [11]. Conducting polymer detachment substantially limits the lifetime and performance of PCMFs and other electroactive materials [12–14] and may trigger inflammation

* Corresponding author. Neural Repair and Biomaterials Laboratory, Hospital Nacional de Parapléjicos (SESCAM), Finca La Peraleda S-N, 45071, Toledo, Spain.
** Corresponding author.
E-mail addresses: miriam.barrejon@uclm.es (M. Barrejón), jcollazos@sescam.org (J.E. Collazos-Castro).

https://doi.org/10.1016/j.carbon.2024.119820
Received 26 August 2024; Received in revised form 18 October 2024; Accepted 10 November 2024
Available online 12 November 2024

accompanied by tissue damage when the immune system becomes exposed to polymer fragments, fostering the development of advanced material engineering strategies to improve its interfacial adhesion.

Increasing the roughness of metallic electrodes and/or using dopants of low molecular weight for PEDOT electro-synthesis enhances the conducting polymer adhesion on platinum, iridium, and their alloys, upgrading their endurance for electrical stimulation [15,16]. Modifying the surface chemistry of the substrate may also enhance polymer adhesion [17–19]. For instance, electrodepositing an initial film of P(EDOT-NH_2) on indium thin oxide or platinum provides an anchoring layer for subsequently electrodeposited PEDOT, which becomes more strongly adhered to the surface [17]. However, the resulting P(EDOT-NH_2) films show no electroactivity and reduce the charge storage capacity and electrical admittance of the underlying metal [17], thus detracting from their usefulness in the fabrication of neural microelectrodes, which are intended to supply electric current at a fast rate, usually in pulses of hundreds of μA with duration of 0.1–0.4 ms [20,21]. Similarly, electrografting diazonium salts on metal electrodes enhances the adhesion of the ensuing PEDOT coating, but greatly reduces the electroactivity of the metal surface [18,19]. Therefore, developing electroactive linkers that covalently bond PEDOT without passivating the underlying substrate is critically needed for the successful deployment of this technology in advanced medical devices.

The intrinsic hydrophobicity and chemical inertness of carbon materials [22,23] significantly contributes to the poor adhesion of the conducting polymer coating, and covalent modification of the carbon surface is a timely approach to overcome this limitation. However, introducing covalent bonds may disrupt the π-conjugated structure responsible for carbon electrical conductivity. Grafting of diazonium salts and related compounds is widely used to tailor the mechanical, chemical, and optoelectronic properties of carbon-based materials, producing strong covalent bonding and robust structures. For instance, reductive linking of aryl diazonium salts or amidation reactions are used for mechanical reinforcement of carbon fiber-based composites [24–26]. Nevertheless, surface modification with diazonium salts comes at the price of disrupting C=C double bonds by converting sp^2 carbon atoms into sp^3 ones, which leads to the destruction of the optoelectronic properties [27,28]. In recent years, the [2 + 1] cycloaddition of electron-poor aromatic nitrenes has been exploited to chemically modify carbon nanotubes without altering the π-conjugated electronic structure [29,30]. This approach initially forms a three-membered ring, which subsequently evolves by opening the bridge, restoring the sp^2 hybridization and recovering the π-conjugated system. As a result, the outstanding electrical conductivity of the original material is preserved. Nitrene derivatives have also been used to functionalize carbon microfibers (CMFs) and facilitate their incorporation in composite materials [31]. The functionalized microfibers showed no deterioration of their mechanical properties, particularly in terms of tensile strength. Hence, covalent chemical modification of CMFs through the [2 + 1] cycloaddition of nitrene derivatives appears as a promising approach to yield fully conjugated hybrid structures with superior electrical, mechanical, and optical properties, appropriate for the design of neurological implants.

Herein, PCMFs with strengthened adhesion of PEDOT and enhanced electric charge transfer are fabricated using electroconducting EDOT linkers. Besides electrical impedance spectroscopy (EIS), biphasic rectangular electric pulses of short duration (200 μs) resembling those used in neuroprosthetics [20,21] are applied for testing the performance of the microfibers. In a first step, novel EDOT derivatives are synthesized and tested for covalent functionalization of CMFs based on aryl diazonium salts chemistry or [2 + 1] nitrene cycloaddition reactions. Both chemical routes result in the formation of an EDOT-based molecular layer anchored to the carbon surface as demonstrated by thermogravimetric analyses (TGA), Raman spectroscopy, and X-ray photoelectron spectroscopy (XPS). Although both types of linkers enable successful PEDOT growth on the CMFs via oxidative electropolymerization, resulting in a robust nanostructured surface architecture, diazonium derivatives drastically impair electric charge transfer. In contrast, nitrene cycloaddition, via aziridine formation, increases the conductivity of the carbon surface and the final PCMFs. This chemical approach also makes the polymer more resistant to detachment upon vibration stress or when implanted into the spinal cord, thereby optimizing their integration into the neural milieu.

2. Experimental section

2.1. Materials and methods

All chemicals were reagent-grade, purchased from commercial suppliers and used as received. Column chromatography was performed on Merck silica gel 60 (ASTM 230–400 mesh). Uninsulated, 7-μm-diameter CMFs (C-00-FB-000122 from Goodfellow, United Kingdom) were used for all the experiments.

Analytical thin layer chromatography (TLC) was performed using silica-coated Merck 60 F254 plates and flash chromatography was performed using silica gel (Scharlab 60, 230–400 mesh). NMR spectra were recorded on a Bruker Avance 400 (^{1}H: 400 MHz, ^{13}C: 100 MHz) spectrometer at 298 K, unless otherwise stated, using partially deuterated solvents as internal standards. Coupling constants (J) are denoted in Hz and chemical shifts (δ) in ppm. Attenuated total reflection Fourier transform infrared (ATR-FTIR) spectra were recorded using an Avatar 370 spectrophotometer within a spectral range of 400–4000 cm^{-1}. Raman spectra were obtained on a Renishaw inVia Raman microscope at room temperature with an exciting laser source $\lambda = 532$ cm^{-1}. Measurements were taken with 10 s of exposure time, and the laser spot was focused on the sample surface using a 50× short working-distance objective and an output power set at 10 %. Thermogravimetric analysis (TGA) was utilized for the characterization of the thermal stability by measuring the weight change as a function of temperature, using a TGA/DSC Linea Excellent instrument by Mettler-Toledo under a nitrogen flow (90 mL/min). The CMF-based materials were cut into small pieces, introduced into a platinum crucible, and heated up to 1000 °C at a heating rate of 10 °C/min. Photoelectron spectra (XPS) were acquired with a PHI VersaProbe II spectrometer equipped with a monochromatic AlKα X-ray source (Al 1486.6 eV mono at 47.3 W). The spectrometer energy scale was calibrated using Cu $2p_{3/2}$, Ag $3d_{5/2}$, and Au $4f_{7/2}$ photoelectron lines at 932.7, 368.3, and 84.0 eV, respectively. The kinetic energies of photoelectrons were measured using a hemispherical electron analyzer working in the constant pass energy mode (High-Resolution Spectra Pass Energy (eV): 29.35; Survey Spectra Pass Energy (eV): 187.85). The residual pressure in the analysis chamber was maintained below 5×10^{-7} Pa during data acquisition, and binding energies (accurate ± 0.1 eV) were determined with respect to the position of the adventitious C 1*s* peak at 285.0 eV.

2.2. Chemical modification of CMFs

2.2.1. General procedure for the synthesis of f-CMF 1-2

A carbon fiber bundle (10 mg) was accurately weighted and added to a round bottom flask with EtOH (25 mL). The corresponding amino derivative (10 mg, 1:1 wt ratio) was added, and the reaction flask was heated to 70 °C in an oil bath. Isoamyl nitrite was then added slowly (0.5 mL), and the mixture was stirred for 24 h. After cooling down to room temperature the final product was filtered and washed with EtOH and CH_2Cl_2 several times, and then dried in a vacuum oven for 24 h.

2.2.2. Synthesis of f-CMF 3

A carbon fiber bundle (10 mg) was accurately weighted and added to a round bottom flask with EtOH (25 mL). Edot-Ph-N_3 (100 mg, 1:10 wt ratio) was added, and the reaction flask was heated to 70 °C in an oil bath for 72 h. After cooling down to room temperature the final product was filtered and washed with EtOH and CH_2Cl_2 several times, and then

dried in a vacuum oven for 24 h.

2.3. Electrical and mechanical characterization of CMFs and PCMFs

Starting and chemically-modified CMFs were used to fabricate 1-mm long electrodes for PEDOT electrodeposition and electrochemical studies. In brief, single microfibers were introduced into borosilicate capillaries (A-M Systems) applying negative pressure. One of the sides of the capillary was sealed with silicone, allowing the CMF to protrude outside. The CMF was then trimmed to a length of 1 mm. At the rear end of the capillary, the CMF was cut, and the internal and external surfaces of the capillary were painted with colloidal graphite (Agar Scientific) to provide adequate electrical connection. A small strip of conductive adhesive tape was placed around this side to allow a firm contact with the clamps of the potentiostat during the performance of all the electrochemical techniques.

PEDOT doped with poly[(4-styrenesulfonic acid)-co-(maleic acid)] (PSS-*co*-MA) was deposited on the 1-mm microfiber tip by galvanostatic electropolymerization at room temperature. An Autolab PGSTAT302 potentiostat/galvanostat (Eco Chemie) was used in three-electrode cell configuration in NaCl-free phosphate buffer (PB) solution containing 15 mM 3,4 ethylenedioxythiophene (EDOT monomer; Sigma-Aldrich) and 20 mM PSS-*co*-MA sodium salt (Sigma-Aldrich). A platinum foil was used as counter-electrode (CE), and an Ag/AgCl electrode (MI-402, Microelectrodes, INC.) was used as reference (RE). A constant anodic current (calculated to provide 1 μA/mm^2, which meant 22.02 nA through the 0.022 mm^2 surface of the 1-mm-long surface of the electrode) was applied for 1920 s (192 mC/cm^2, for a total charge of 42.275 μC) while recording the electrode potential every second. The Autolab potentiostat was likewise used for EIS and for measuring electric current during rectangular electric pulse application in the same NaCl-free PB electrolyte. Cyclic voltammetry (CV) was used to confirm the correct polymer deposition. With the electrode configuration described before, the voltage of the microfibers with or without polymer was swept at 50 mV/s, from −0.5 to +0.55 V, while the current response was recorded at potential intervals of 20 mV. Electrochemical tests were performed in a custom-made mini-electrochemical cell designed to reduce the volume of the electrolyte and minimize charge dispersion. The cell had a hollow a hollow cylindrical shape (2.5 mm inner diameter, 3.5 mm outer diameter, 22 mm length), with a 2 mm-diameter Ag/AgCl electrode (MI-402) placed in one edge as RE. A platinum wire (0.127 μm diameter), coiled around the base of the RE shaft, acted as CE. Finally, this side of the cylinder was sealed with silicone to make it watertight. Two lateral tubes were connected to the cylinder near the RE side to allow refilling with PB if necessary. The CMF-based electrodes to be tested were individually introduced through the opposite side, with the tip of the electrode facing the RE at a distance of 2 mm. For EIS, 20-mV sine waves were applied at 26 logarithmically spaced frequencies from 10^5 to 1 Hz through the microfibers. For chronoamperometry, trains of ten consecutive biphasic, cathodic-first, 200-μs-width voltage pulses were applied at 0.1, 0.2 and 0.3 V through the microfibers while recording their current responses at 10^3 kHz sampling rate. The total charge per pulse was calculated by integrating and adding the cathodic and anodic currents in absolute value along time.

To evaluate the mechanical behavior of the conducting polymer coating on CMFs, controlled vibration stress was applied to the microfibers and electrical measurements were taken periodically as a correlate of the coating stability. The 1-mm long microfiber-based electrodes were individually fixed by a screw to a grooved holder connected by a bolt to the vibrating block of a Leica-VT1000S vibratome. Vibration at 80-Hz was applied with the microfiber tips immersed into artificial cerebrospinal fluid solution (ACSF), whose composition was (in mM): NaCl 120, KCl 2.5, NaH_2PO_4 1.0, $MgCl_2$ 1.2, $CaCl_2$ 2.5, $NaHCO_3$ 26.2, glucose 11, pH 7.4 when equilibrated with 95 % O_2/5 % CO_2. Vibration was paused at some time points (30 s and 1, 2, 5 and 10 min) and the microfiber electrodes were collected for electrochemical tests (EIS and chronopotentiometry) in the minicell. Chronopotentiometry consisted of three symmetric biphasic pulses administered at 300 Hz, while voltage was monitored at 10^3 kHz. The pulses were square waves, cathodic-first 200 μs/50 μA per phase, with a 20-μs zero current (i = 0) interphase between the cathodic and anodic voltages. Cathodic and anodic polarizations were measured immediately after each phase when the current intensity was zero.

Scanning electron microscopy was used to acquire images of PCMFs after the vibration stress protocol. For this, a FEI Verios 460 microscope in high-vacuum mode and using a “through the lens” detector was employed at 2 kV. Due to the conductive nature of CMFs and PCMFs, no additional metallic covering was needed for visualization.

2.4. Testing PCMFs in vivo

The experimental protocols adhered to the recommendations of the European Commission and the Spanish regulations for the protection of experimental animals (86/609/CEE, 32/2007, and 223/1988) and were approved by the local Ethics Committee for Animal Experimentation (approval number 227BCEEA/2023). Adult male Wistar rats (12 weeks old, 300–320 g) raised at the animal facility of the Hospital Nacional de Paraplejicos (Toledo, Spain) were used. Rats were housed in groups of two at a 12 h light/dark cycle with food and water available ad libitum. All surgical procedures were performed under general anaesthesia with intraperitoneally applied sodium pentobarbital (55 mg/kg) mixed with atropine (0.025 mg/kg) and xylazine (5 mg/kg), administering a 30 % supplemental dose of these drugs when needed. An unguent was applied to the eyes to prevent corneal abrasion and infection. Animals were kept at 37 °C with the aid of a thermal pad. Antibiotic (enrofloxacine, 0.1 mL/kg) was administered subcutaneously immediately after surgery and daily for one week. Analgesic (meloxicam, 25 mg/kg) was also administered after surgery and at 8 and 16 h later.

The procedures for PCMFs modification with biomolecules and implantation in the uninjured rat spinal cord have been reported elsewhere [8,9]. Briefly, PCMFs were sterilized by formaldehyde gas and then covered with poly-L-lysine (Sigma-Aldrich, P2636), heparin (Sigma-Aldrich, H5515), recombinant human bFGF (R&D, 4114-TC-01 M), and bovine fibronectin (Sigma-Aldrich, F1141). Subsequently, they were repetitively rinsed with sterile distilled water, dried and used for implantation. The spinal cord segments T10-11 were surgically exposed and a small cut was made with microscissors in the dura mater. Individual PCMFs (1.8 mm long) were introduced from dorsal to ventral into the spinal cord, at approximately 0.5 mm from the midline and separated at least 0.5 mm in the longitudinal plane (Fig. 7a). The muscle planes were sutured, and the skin was closed with metallic clips. Two groups of animals received control (washed, non-functionalized PCMFs) or washed, aziridine-functionalized PCMFs. Four animals were used per group, each animal receiving 4–7 MFs. Microfibers that were in contact with the ventral dura matter were excluded from cellular analyses because this facilitated invasion of meningeal cells into the neural tissue.

Three months after microfiber implantation, the animals were transcardially perfused with isotonic saline followed by 4 % paraformaldehyde in 0.1 M, pH 7.4 phosphate buffer (0.8 mL of perfusion solution per gram of body weight). The spinal cord was removed, immersed in 30 % sucrose for 48 h and processed for histology. To assess the optimal methods for histological processing and quantification, the spinal cord was cut in horizontal sections for two animals of each group, and in transverse sections for the other two. Quantifications are shown only for the spinal cords cut in the transverse plane because this allowed an optimal preservation and identification of the microfibers. Therefore, methodological descriptions are only provided for this case. In brief, transverse 60-μm spinal cord sections were cut with a cryostat and incubated for 1 h in 0.1 M, pH 7.4 PBS containing 0.2 % Triton, rinsed with PBS and then incubated for 2h in PBS with 0.2 % Triton with NeuroTrace™ fluorescent Nissl stain (Molecular Probes, N-21479) at concentration 1:60 and Hoechst 33342 (Molecular Probes, 1.5 mg/mL).

Finally, the sections were rinsed and mounted with Immuno Mount™ and processed for microscopy. Mosaic images of tissue sections were captured with an Olympus 1X83 microscope equipped with a 10x objective and a digital camera (Orca-Flash 4.0, CellSens Dimension software). Mosaics were imported into the QuPATH software, and the regions of interest (i.e., the microfibers and tissue in the nearby 10-μm) were further processed with the Image J software for cell nuclei counting. In the same images, the length of the microfiber with signs of polymer detachment was measured and expressed as percentage of the microfiber length. Additionally, the tissue sections were imaged using a confocal laser-scanning microscope. Z-stacks of images taken each 0.5 mm were acquired with a 63x-objective and 3.5 zoom for a better visualization of the PCMFs and the cellular elements within the tissue.

3. Results and discussion

3.1. Chemical modification of CMFs and characterization of the resulting materials

For the sake of comparison, CMFs surface modification is accomplished via two different chemical strategies, namely aryl diazonium salt chemistry from the corresponding amino derivatives, or [2 + 1] nitrene cycloaddition generated *in situ* from the corresponding azides. These chemical strategies are aimed at evaluating different physicochemical paradigms: i) through the incorporation EDOT-Ph and $EDOT_2$-TPA moieties via diazonium salts chemistry (top and middle routes in Scheme 1), the effect of introducing highly conjugated molecules, such as TPA, in the final electrical properties of the hybrid materials is studied; and ii) the effect of using different types of chemical anchors (i.e. carbon-carbon bonds or three-membered aziridine rings) to covalently attach the polymer. To implement these approaches, three EDOT derivatives are prepared (Scheme 1, left part) and anchored onto the carbon surface. The amino derivatives (EDOT-Ph-NH_2 and $EDOT_2$-TPA-NH_2 in Scheme 1) are synthetized adapting the chemical procedures described in the literature [32–35], as further described in the experimental section of the supporting information and Scheme S1 (characterization data is given in Figs. S1–S5, supporting information). The as-prepared amino derivatives are covalently attached to the CMFs surface by reacting the different amines with the CMFs in ethanol for 24 h in the presence of isoamyl nitrite. Purification of the functionalized CMFs is performed by the common washing/filtration/sonication workup procedure to yield *f*-CMF 1 and *f*-CMF 2 (Scheme 1). As a next step, the azido derivative EDOT-Ph-N_3 is synthesized from the corresponding amine by modifying a published procedure [36] and the resulting azide is characterized (Figs. S1–S5) and employed for covalent modification of the CMFs via [2 + 1] nitrene cycloaddition, that, after the washing/filtration/sonication workup procedure, yields aziridine-functionalized CMFs, hereinafter referred to as *f*-CMF 3 (Scheme 1, bottom).

The first evidence of successful covalent modification of the CMFs is obtained from thermogravimetric analysis (TGA), consisting of heating ramps of 10 °C/min up to 1000 °C, performed under nitrogen flow (Fig. 1). The starting CMFs present no significant weight loss between room temperature and 1000 °C. In contrast, the functionalized CMFs show gradual decomposition as the temperature raises. The weight losses (wt %) measured for the thermal decomposition of the modified CMFs at 750 °C are 17.1 % for *f*-CMF 1, 24.2 % for *f*-CMF 2, and 19.5 % for *f*-CMF 3, compared to 3.6 % of the starting CMFs, demonstrating the existence of the EDOT-based anchoring layer on the surface of the CMFs. Furthermore, the degree of surface functionalization of carbon-based materials significantly influences their final properties. Therefore, achieving comparable levels of functionalization is crucial for this study, especially for those CMFs bearing similar molecular structures (i.e. *f*-CMF 1 and *f*-CMF 3), as this enables a more accurate comparison of their physicochemical properties. The above percentages have been used to estimate the loading of functional groups (FGL) onto the surface of the CMFs in mmol/g, calculated according to Equation (1) described in the literature [37–39], and the results confirm the presence of rather similar FGL for *f*-CMF 1 and *f*-CMF 3 (Table 1).

$$FGL = \frac{\text{wt \%} \times 1000}{\text{Mw}\,(100 - \text{wt \%})} \quad (1)$$

where wt % is the weight loss percentages measured for the thermal decomposition of EDOT derivatives at 750 °C and Mw is the molecular weight for each EDOT derivative.

The Raman spectra of the starting CMFs and the functionalized CMFs (*f*-CMF 1–3) are shown in Fig. 2. The spectrum of the starting CMFs shows two characteristic peaks, which are assigned to the graphitic E_{2g} G mode at ~1590 cm^{-1} and the disorder D mode at ~1365 cm^{-1} [40–42]. The latter represents the conversion of C atoms from the sp^2 to the sp^3 hybridization state, thereby providing information about the structural disorder and the changes in the π-conjugated framework of the carbon

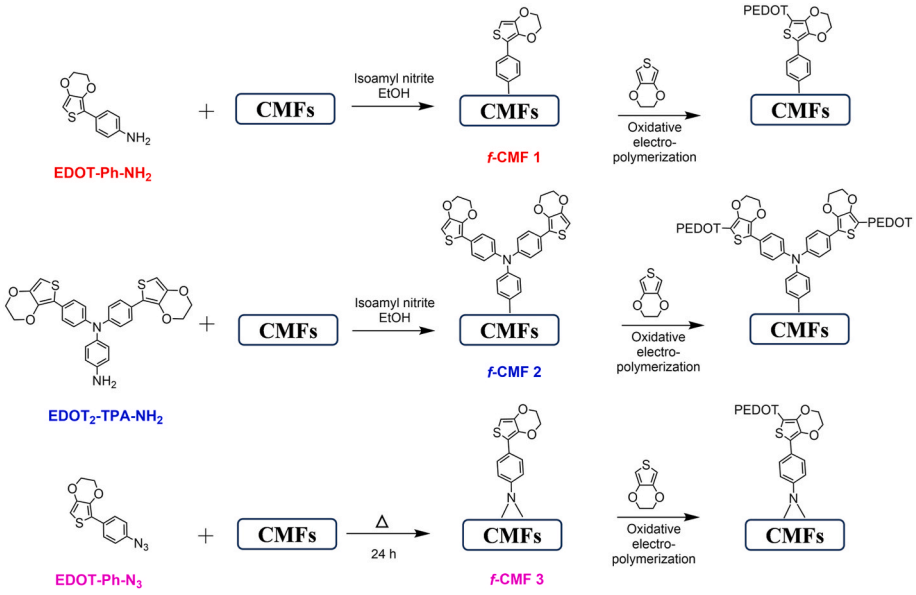

Scheme 1. Synthetic pathways for the covalent chemical modification of CMFs.

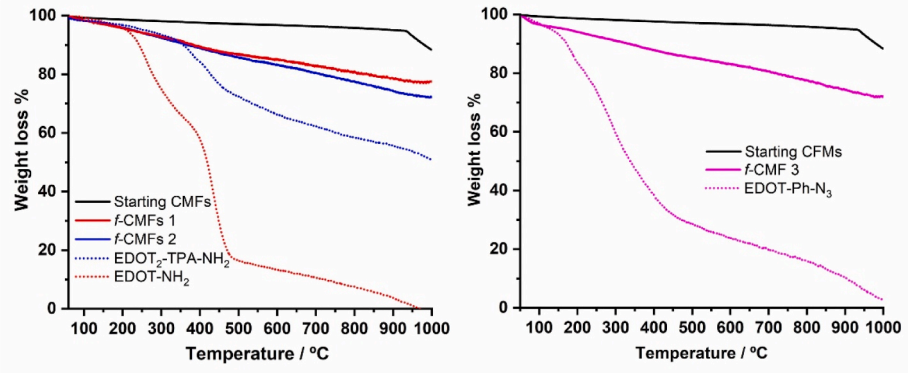

Fig. 1. TGA curves for *f*-CMF 1 and *f*-CMF 2 (left), and *f*-CMF 3 (right), compared to the starting CMFs and the corresponding EDOT derivatives under N_2 atmosphere. (A colour version of this figure can be viewed online.)

Table 1
Weight loss percentages and loading of functional groups (FGL) on the CMFs.

MATERIAL	Wt %	FGL (mmol/gr)[a]
Starting **CMFs**	3.6	–
***f*-CMF 1**	17.1	0.89
***f*-CMF 2**	24.2	0.61
***f*-CMF 3**	19.5	0.98

[a] mmol of functionalizing groups per gram of material.

surface. Thus, the relative intensity of the D-band to the G-band (I_D/I_G ratio) demonstrates the successful covalent functionalization of the CMFs due to the surface treatment. The higher I_D/I_G of the functionalized materials as compared to the starting CMFs suggests a higher number of functional groups on the surface of the CMFs. When the chemical modification is accomplished via aryl diazonium salts chemistry, the I_D/I_G ratio increases from 0.92 to 0.96 for *f*-CMF 1 and to 0.98 for *f*-CMF 2, due to the introduction of sp^3 defects through carbon-carbon covalent bond formation (Fig. 2, left). However, as already mentioned, the [2 + 1] cycloaddition of nitrene derivatives occurs without the disruption of the carbon sp^2 network, and consequently there is no increase in the I_D/I_G ratio when moving from the starting CMFs to *f*-CMF 3 (Fig. 2, right). This clearly evidences the preservation of the π-conjugated electronic structure after covalent anchorage of the EDOT derivatives via aziridine formation.

XPS has been used to further identify the presence of EDOT moieties on the surface of the CMFs. The XPS survey spectra of functionalized CMFs in comparison to the starting CMFs are shown in Fig. 3a. The survey spectrum of the starting CMFs shows carbon and oxygen peaks as major constituents; however, other major elements such as nitrogen and silicon are also present on the CMFs, probably originating from the manufacturing process. After covalent chemical modification through the afore-mentioned approaches, two relevant sulfur signals (S2p and S2s, highlighted in red in Fig. 3a) appear as low-intensity peaks in all the functionalized materials (*f*-CMFs 1–3). This is the most direct evidence of the EDOT derivatives anchored to the microfibers. The percentages for each chemical element are summarized in Table S1 (supporting information). The high-resolution S2p XPS spectra (Fig. 3b–c) display the typical spin-split sulfur coupling $S2p_{3/2}$ and $S2p_{1/2}$ in the range of 160–167 eV. The additional signals appearing at higher binding energies (167–169 eV) can be attributed to oxidation products, likely resulting from partial oxidation of the sulfur in the thiophene ring [43]. Finally, the chemical shifts observed for both S2p components ($S2p_{1/2}$ and $S2p_{3/2}$) following the covalent modification of the CMFs, compared to the free precursor EDOT derivatives, indicate changes in the chemical environment. These shifts can be attributed to the formation of covalent bonds between the EDOT derivatives and the surface of the CMFs [44].

3.2. Charge transfer and PEDOT electropolymerization in f-CMFs

Bonding the EDOT-based linkers to the CMFs induces no significant changes on their open circuit potentials (Fig. 4b, upper panel), indicating that the three types of *f*-CMFs remain grossly similar regarding their electrochemical reactivity in the liquid electrolyte. However, *f*-CMFs 2 show a drastic reduction in electric charge transfer, reaching only between 35 % and 38 % of that of the starting CMFs for the 200-μs pulses of 0–1 to 0–3 V (Fig. 4g), and also increase their electrical impedance at low and medium frequencies (Fig. 4j). *f*-CMFs 1 become less impaired electrically but still lose charge transfer ability after the functionalization (Fig. 4f), whereas *f*-CMFs 3, functionalized with

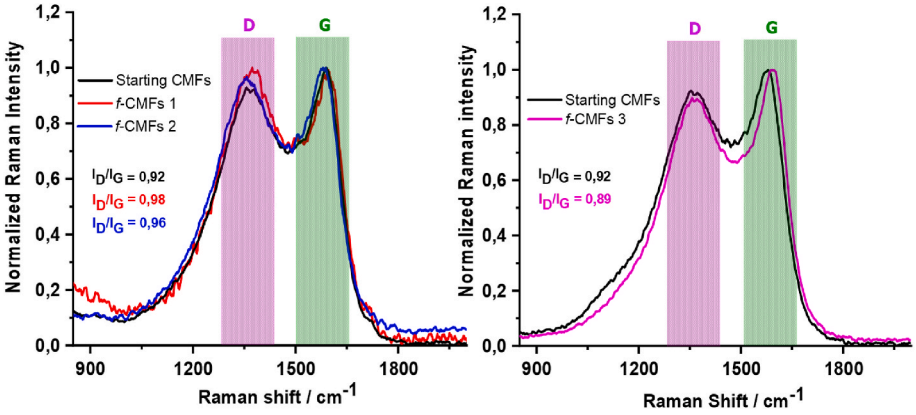

Fig. 2. Raman spectra for *f*-CMF 1 and *f*-CMF 2 (left), and *f*-CMF 3 (right) compared to the starting CMFs (black line). Laser line: 532 nm. (A colour version of this figure can be viewed online.)

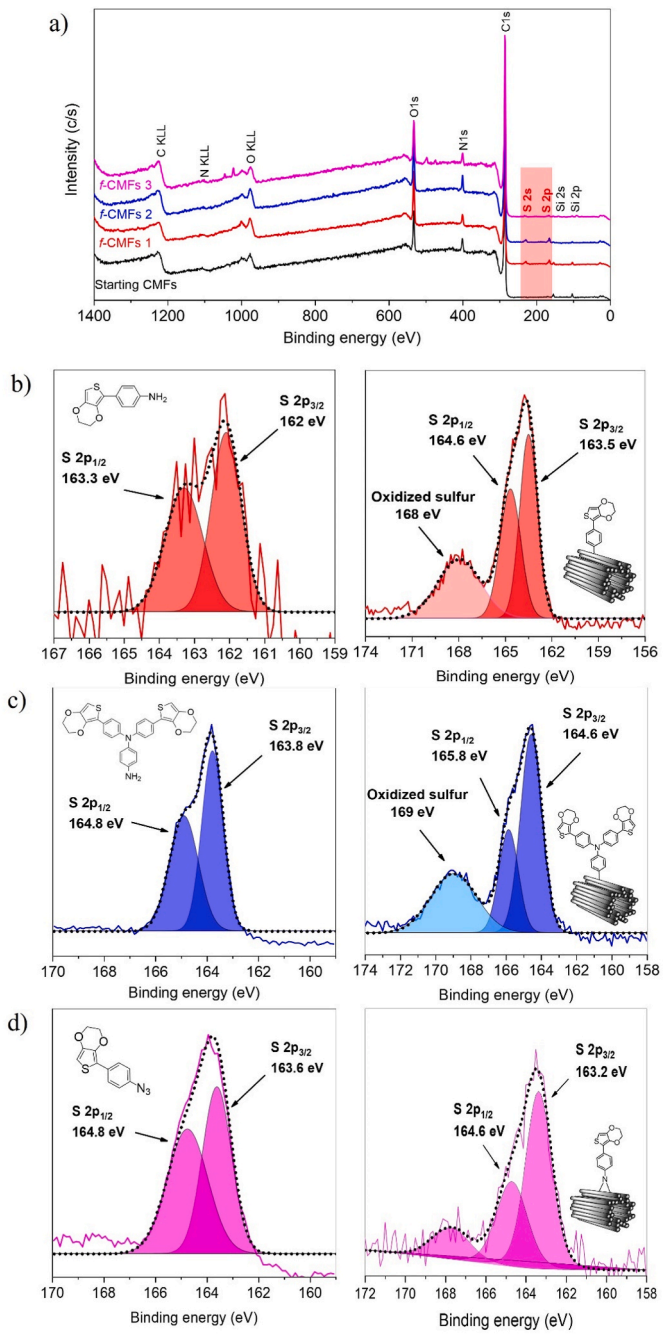

Fig. 3. a) Stacked X-Ray photoelectron survey spectra for the functionalized CMFs compared to the starting CMFs; b), c), and d) high resolution XPS spectra for *f*-CMFs 1–3 (right) and their corresponding precursor molecules (left). (A colour version of this figure can be viewed online.)

aziridine, are not impaired at all and tend to reduce their electrical impedance instead (Fig. 4h–k). These results are in agreement with the Raman spectroscopy characterization and suggest that the marked worsening of charge transfer in *f*-CMFs 2 results from the additive effects of distorting the carbon graphite-like lattice when adding covalent bonds, as reported for other carbon materials [27,45,46], together with the presence of the neutral TPA molecule itself, which has a relatively large bandgap (4.65 eV) that hinders electric conduction [47,48].

Notwithstanding the abovementioned differences in the electrical behavior of the *f*-CMFs, PEDOT can be successfully electropolymerized on all fiber types by galvanostatic method (Section 2), reaching a voltage plateau between 0.86 and 0.90 V soon after starting the polymerization (Fig. 4a). A slight but reproducible and maintained increase in the voltage measured during polymerization occurs in *f*-CMFs 2 compared to starting (non-functionalized) CMFs, suggesting that the TPA linker certainly provides an electrical pathway of higher resistance to current flow from the carbon surface to the PEDOT chains (Fig. 4b, lower panel). Further proof of successful conducting polymer deposition on the different CMFs is given by cyclic voltammetry (CV), a technique commonly used to assess the electrochemical properties of electrodes. The large increase in CV area and the associated redox processes (Fig. 4c–e) are characteristic of PEDOT:PSS-*co*-MA [49]. Moreover, the PEDOT coating substantially enhances the electric capacitance of the microfibers, similarly to other PEDOT-coated carbon fiber electrodes [50,51]. Despite the successful polymer deposition in all microfibers, CV also evidences a lower charge storage capacity in PEDOT-coated *f*-CMFs 1 and 2 compared to *f*-CMFs 3.

For all *f*-CMFs, adding the conducting polymer coating increases 2–3 times the charge supplied per voltage pulse (Fig. 4f,g,h and Figure S6a,b,c) and reduces the electrical impedance 2-3 orders of magnitude, mainly at medium and low frequencies (Fig. 4i,j,k). Despite this, PEDOT coated *f*-CMFs 1 and *f*-CMFs 2 still yield about 49 % and 70 % of total charge per pulse and have higher impedance than starting PCMFs; whereas PEDOT-coated *f*-CMFs 3 match the starting PCMFs in both parameters. Thus, CV, EIS and chronoamperometry measurements indicate that CMF functionalization via diazonium salts impairs the interfacial electrical coupling of PEDOT electrodeposited on the carbon surface, whereas aziridine functionalization seems optimal to covalently anchor PEDOT while preserving the electric charge transfer capacity at the interphase.

3.3. *Mechanical correlates of carbon-PEDOT covalent bonding*

The adhesion of the developed nanostructured surface in the functionalized CMFs is evaluated through a series of studies. *f*-CMFs 1 and *f*-CMFs 2 are ruled out as promising candidates for the intended application and the adhesion of the conducting polymer is assessed only on *f*-CMFs 3. Starting PCMFs and *f*-PCMFs 3 are submitted to mechanical vibration at 80 Hz, and electrical data (charge per pulse and electrochemical impedance) together with SEM imaging are used as functional and morphological correlates of the resistance of the PEDOT coating to rupture and detachment from the microfibers. Vibration tests are useful to study the electrical parameters as well as the elastic stability of carbon-based electrodes [52]. Here, the microfibers are immersed in a solution of artificial cerebrospinal fluid (ACSF) during the test to partially mimic the neural tissue environment. Maximum cathodic (E_{mc}) and anodic (E_{ma}) polarization potentials produced by the application of cathodic-phase-first biphasic current pulses, and electrochemical impedance, which are inversely correlated with the presence of the polymer on the microfibers, are measured at different times of vibration (Section 2). The test is finished when voltage surpasses the electrochemically safe values for PEDOT:PSS-*co*-MA (−0.9 to +0.55 V) [6], because this will preclude the usefulness of the microfibers as stimulating electrode *in vivo* [53].

E_{mc} produced by the polymer-coated microfibers progressively increases with vibration time (Fig. 5a). The starting PCMFs reach the potential limit of −0.9 V during the first minutes of vibration and fully overpass this value by 10 min. However, E_{mc} evolves more slowly and remains within the 0.9 V-limit in PEDOT-coated *f*-CMFs 3 (Fig. 5a), indicating a higher adhesion of the PEDOT layer. In pace with the higher cathodic polarization, a progressive increase in the impedance modulus is observed in starting PCMFs at low frequencies, becoming about one order of magnitude higher at 1–10 Hz by the end of the 10-min vibration (Fig. 5b). In sharp contrast, impedance of PEDOT-coated *f*-CMF 3 barely increases during the same time (Fig. 5c). IES spectra of the two kinds of microfibers are directly compared in Fig. 5d at 0, 2, and 10 min of vibration. Statistically significant differences, with lower electrochemical impedance due to the chemical modification of the CMFs surface, are found after 10 min of vibration along the frequencies from to 2.5

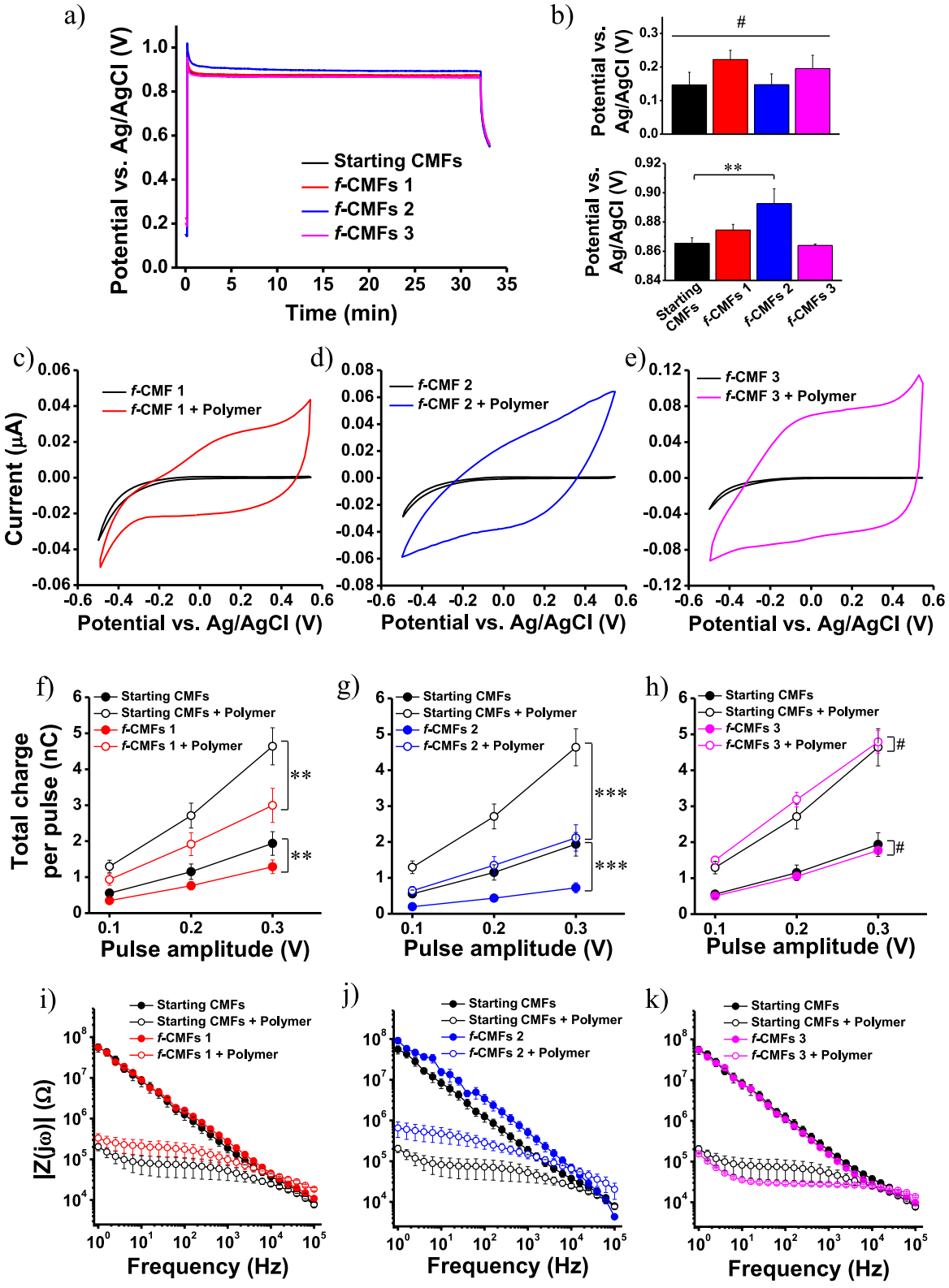

Fig. 4. a) Voltage recorded during PEDOT:PSS-*co*-MA polymerization in starting CMFs and chemically modified CMFs. Anodic current of 1 μA/mm^2 was applied for 1920 s. b) Open circuit potential of the microfibers measured before (upper panel) and along the last minute (lower panel) of the polymerization process. p (ANOVA) ** < 0.01 c-e) Cyclic voltammetry diagrams obtained from *f*-CMFs 1 (c), *f*-CMFs 2 (d) and *f*-CMFs 3 (e) before and after PEDOT:PSS-*co*-MA electrodeposition. f-h) Total charge per pulse (cathodic plus anodic) recorded during the application of voltage pulses of the indicated amplitudes through the different microfibers, before and after polymer deposition. p (two-way ANOVA) ** < 0.01; *** < 0.001; # No statistically significant differences. i-k) Bode plots from EIS measurements for the same microfibers. n = 11 or 12 for each type of CMFs. All data are expressed as mean ± standard errors. (A colour version of this figure can be viewed online.)

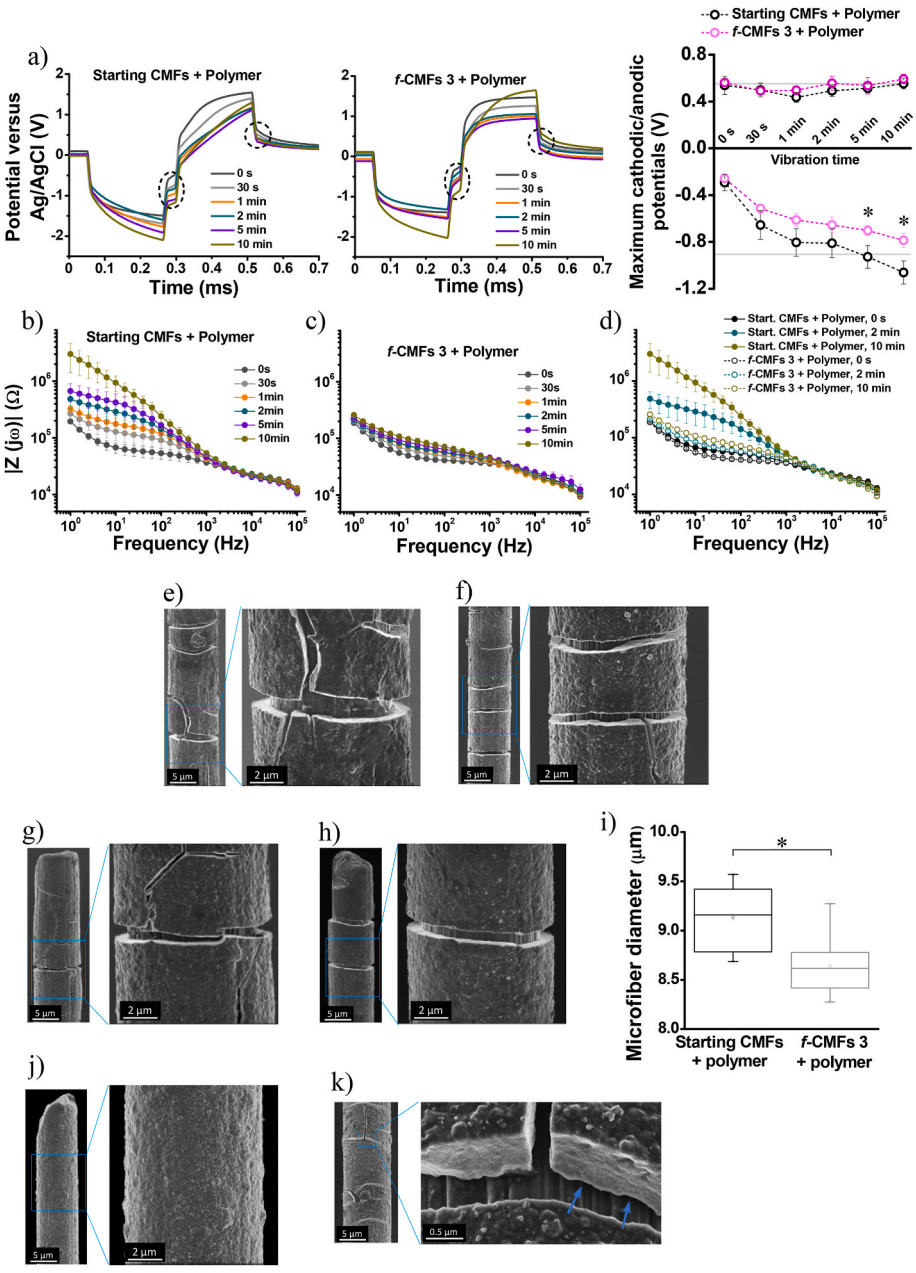

Fig. 5. a) Voltage transients evoked by application of biphasic current pulses of −50/+50 μA to starting PCMFs (left panel) or PEDOT-coated *f*-CMFs 3 (middle panel) at the indicated times of vibration mechanical stress. The right panel illustrates the maximum cathodic and anodic polarization potentials obtained from the traces in the left and middle panels (indicated by the dashed ovals and circles). b) EIS Bode plots of starting PCMFs at the time points shown in a), left panel. c) EIS plots of PEDOT-coated *f*-CMFs 3 at the time points shown in a), middle panel. d) Comparison of EIS data from starting PCMFs and modified PEDOT-coated *f*-CMFs 3 at 0, 2 and 10 min of vibration. All data are expressed as mean ± standard errors. e-h) SEM microphotographs of the surface of representative microfibers after the vibration test. e) Starting PCMF, shaft. f) PEDOT-coated *f*-CMF 3, shaft. g) Starting PCMF, tip. h) PEDOT-coated *f*-CMF 3, tip. i) Assessment of electrode diameter in a total of $n = 6$ starting PCMFs and $n = 7$ PEDOT-coated *f*-CMFs 3. Box chart indicates median, quartiles and min-max values. *$p < 0.05$ (ANOVA). j) SEM images of an intact PCMF, not submitted to mechanical stress, for visual comparison. k) Detailed example of the gap (arrows) between the polymer coating and the underlying carbon surface in a microfiber after the mechanical stress. (A colour version of this figure can be viewed online.)

Hz–251.2 Hz confirming the enhanced mechanical stability of the PEDOT coating on *f*-CMFs 3.

Besides the electrochemical impedance modulus, phase angle at low frequencies is a reliable parameter to follow-up the degradation and detachment of PEDOT coatings from carbon materials [11,54]. Phase angle progressively deviates in vibrated non-functionalized PCMFs and is much more stable in *f*-PCMFs 3 (Fig. S7). In agreement with the impedance modulus increase, the phase angle progressively diminishes by approximately 27° (from 66.6° to 39.7°) at 1 Hz in starting PCMFs (Fig. S7a), indicating a continued loss of diffusional pseudo-capacitance because of PEDOT detachment from the microfibers. In *f*-PCMFs 3, phase angle decreased only 14.2° at 1 Hz, from 68.6° to 54.4° (Fig. 7Sb), suggesting that the polymer coating remained to a great extent adhered and electrically coupled to the carbon surface. More interestingly, phase angle increased with vibration by 36.6° at 100 Hz in the starting PCMFs (Fig. S7a), compared to only 9.1° increase for *f*-PCMFs 3 (Fig. S7b). Because the impedance modulus was higher after vibration, the increase in phase angle at 100 Hz likely reflects the degree of PEDOT delamination, which will progressively enhance the contribution of the carbon double layer capacitance to electric charge transfer.

Vibration produces visible damage on the nanostructured surface as demonstrated by SEM imaging. Cracks and fissures appear in the polymer coating in both the starting PCMFs and PEDOT-coated *f*-CMFs 3 (Fig. 5e–h). Lesser integrity of the polymer layer, with extensive transverse and longitudinal cracks, as well as polymer separation from the carbon surface, is commonly observed in non-functionalized PCMFs after submitted to vibration (Fig. 5e). PEDOT-coated *f*-CMFs 3 show few longitudinal fissures, and the polymer is better preserved and most frequently remains in close contact with the carbon surface (Fig. 5f), although accurate quantification of this observation is extremely difficult on SEM images.

Nevertheless, when PEDOT separates from the carbon surface, it creates a space at the interphase (Fig. 5k) that eventually increases the total microfiber diameter [11]. The latter parameter reliably indicates that polymer detachment occurs to a greater extent when no carbon surface functionalization is performed. Measured close to the tip, the diameter of PEDOT-coated *f*-CMFs 3 submitted to vibration stress (Fig. 5h) is significantly smaller than that of PCMFs (Fig. 5g) (8.64 ± 0.12 μm vs. 9.13 ± 0.14 μm, respectively, $p < 0.05$, Fig. 5i), and is quite similar to intact, non-vibrated PCMFs (8.52 ± 0.43 μm, Fig. 5j).

The above-mentioned SEM imaging observations support the interpretation that a higher dissociation of the PEDOT coating from the carbon surface is responsible for the large impedance increase in non-functionalized PCMFs submitted to mechanical stress. Taken together, EIS and SEM data indicate that PEDOT covalent bonding to CMFs, mediated by aziridine, results into an intimate interfacial contact with sufficient adhesive strength to resist the mechanical stress imposed by vibration in liquid solutions.

3.4. Controlling for non-covalent CMFs-PEDOT electrical interfacing

PEDOT:PSS-*co*-MA is non-covalently bonded to the carbon surface in the starting PCMFs and still electric charge is successfully transferred through the composite material. Electrostatic and/or hydrophobic interactions likely keep the polymer in close contact to the carbon surface, thus enabling charge transfer. Therefore, it is expected that the chemical composition of the carbon surface substantially influences electron mobility at the interphase [53,55,56]. In addition to carbon and oxygen, heteroatoms like Na, Si, Ca, S, and N are found in CMFs [55,57,58]. Some of those atoms have been identified by XPS in the fibers used in the present study (Fig. 3a and Table S1) and might influence their electrical behavior. Additionally, contaminants physiosorbed onto the microfiber surface during storage and handling [59] may disturb the interfacial coupling. Therefore, to better understand the role of the engineered electroactive linker versus non-covalent interactions in the final electrical properties of the PEDOT-coated *f*-CMFs 3, an additional experiment is performed where the microfibers are washed before the chemical modification. The CMFs are cleaned by a two-step procedure consisting of washings in fresh Milli-Q water followed by HPLC ethanol. To achieve a more effective cleaning, the process is accomplished in an ultrasonic bath for 10-s periods. Subsequently, the washed materials are dried in a vacuum oven and used for the [2 + 1] nitrene cycloaddition reaction to yield aziridine functionalized CMFs. The washing procedure itself significantly reduces electric charge transfer in CMFs (compare Fig. 4e with Fig. 6c). For instance, for a 0.3 V/200-μs pulse, non-coated washed microfibers yield only 1.20 ± 0.24 nC compared to 1.94 ± 0.33 nC for the starting, non-washed counterparts (two-way ANOVA, $p < 0.05$). Moreover, although PEDOT is successfully deposited on both types of microfibers, washed PCMFs produce only 44 % charge per pulse compared to the starting (non-washed) material (2.06 ± 0.36 nC vs. 4.64 ± 0.52 nC, respectively (Two-way ANOVA $p < 0.001$). These results suggest that soluble molecules in CMFs play a relevant role in their electrical conductivity before and after PEDOT coating. Nevertheless, azido-EDOT functionalization allows for a remarkable electrical improvement of washed PCMFs. The voltage recorded at open circuit and during PEDOT electropolymerization is similar for washed microfibers with or without aziridine modification (Fig. 6a and b). However, PEDOT coating of washed *f*-CMFs 3 increases by 317 % the charge produced during 0.3 V pulsing (1.14 ± 0.09 nC vs. 3.62 ± 0.23 nC before and after coated with PEDOT, respectively, $p < 0.001$); whereas

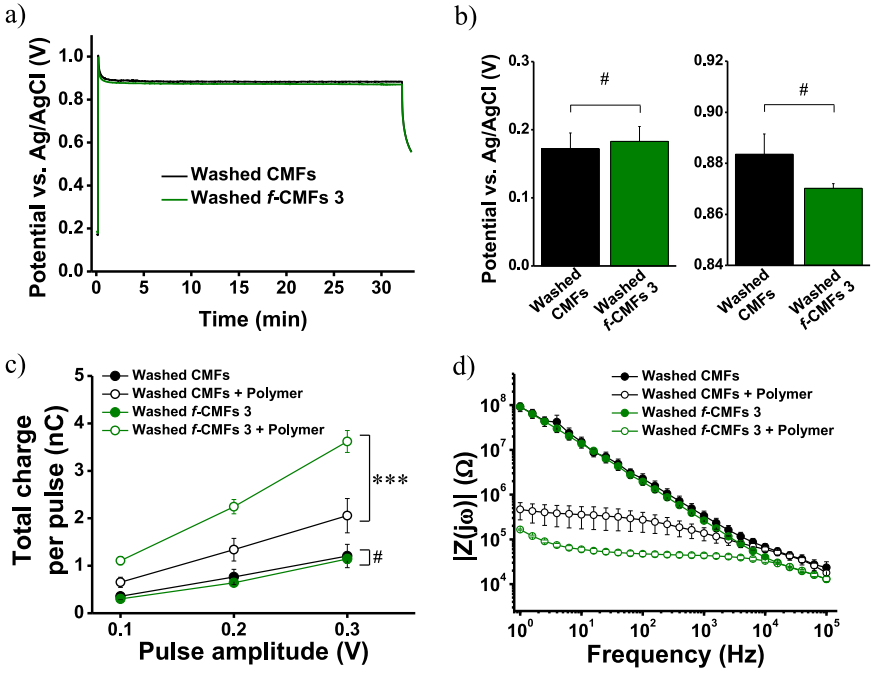

Fig. 6. a) Polymerization curves obtained for washed CMFs and washed *f*-CMFs 3. b) Electric potential of both microfiber types at open circuit (left panel) and during PEDOT electrodeposition last minute (right panel). c) Total charge per pulse (cathodic plus anodic) produced during the application of voltage pulses of the indicated amplitudes through washed, non-coated or washed, PEDOT-coated microfibers. d) EIS Bode plots for the same microfibers shown in c). Averages are from $n = 9$ washed CMFs, $n = 11$ washed-*f*-CMFs 3. p (two-way ANOVA) *** < 0.001 # Not statistically significant differences. All data are expressed as mean ± standard errors. (A colour version of this figure can be viewed online.)

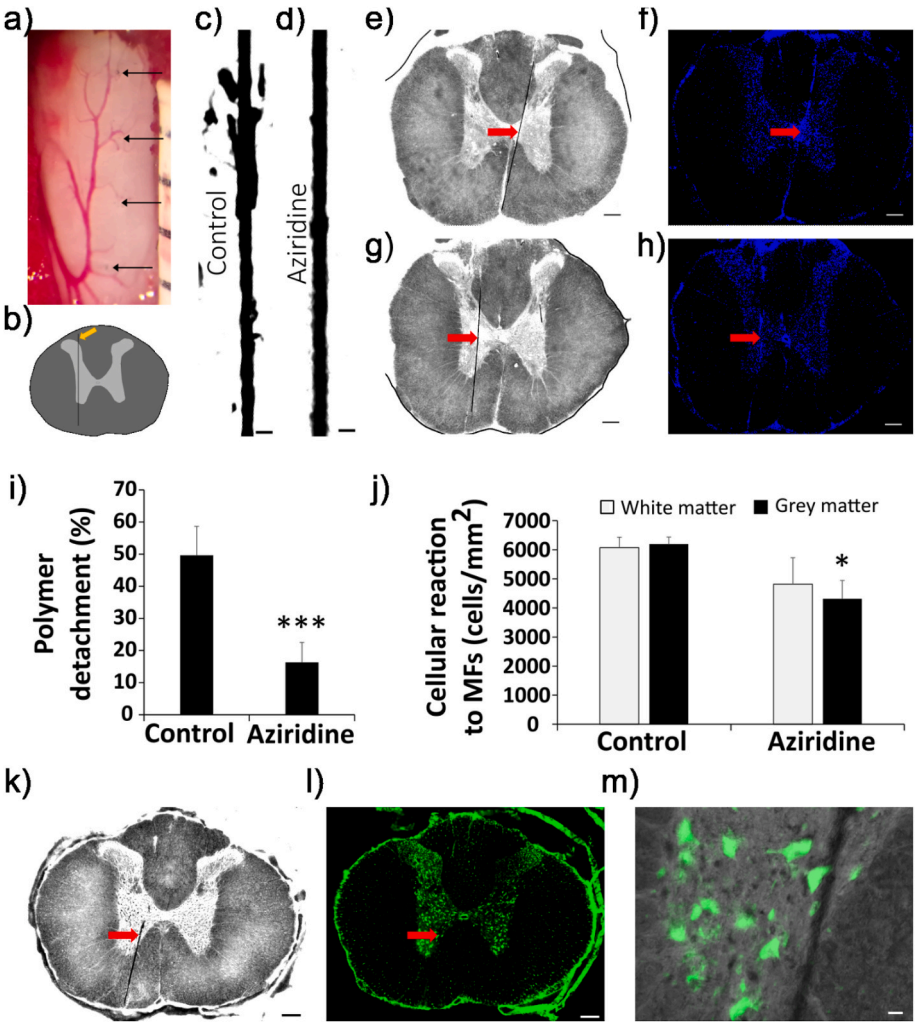

Fig. 7. a) Surgical photograph illustrating some sites of entrance of the PCMFs after their insertion into the spinal cord. b) Drawing depicting the transverse aspect of the rodent spinal cord and the intended location of the microfibers. c) And d), reflected-light confocal microscopy images of microfibers after three months of implantation within the spinal cord, exemplifying extensive PEDOT detachment from the washed non-functionalized (i.e. control) CMFs (c), whereas the coating largely remains adhered to the washed, aziridine-modified (*f*-CMFs 3) microfibers (d). e – h) Cellular reactivity to control (e, f) or *f*-CMFs 3 (g, h) microfibers. Microfiber location within the spinal cord is visualized by transmitted light microscopy (e, g), and reactive cells are labelled using Hoechst fluorescent nuclear staining (f, h). i) Quantification of PEDOT detachment from the CMFs, expressed as percentage of microfiber length. Six microfibers were analysed in the control group and seven for *f*-CMFs group. j) Quantification of reactive (mostly scarring) [9] cells closely associated to the microfibers, considering those in the white and the grey matter separately. k-m) Photomicrographs illustrating the excellent integration of PEDOT-coated, washed *f*-CMFs 3 chronically implanted into the spinal cord, combining transmitted light imaging (k) with NeuroTrace™ fluorescent staining (l) to obtain merged images as that shown in (m). There is not visible disruption of the spinal cord architecture, and healthy neurons (green fluorescent) are in the vicinity and even touch the microfibers. *$p < 0.05$ (ANOVA).

in washed, non-functionalized microfibers, the respective increase is limited to 72 % (1.20 ± 0.24 nC vs. 2.06 ± 0.36 nC, $p < 0.001$) (Fig. 6c). Additionally, PEDOT-coated washed *f*-CMFs 3 show lower electrical impedance compared to those without functionalization (Fig. 6d), confirming the suitability of this covalent chemistry approach to produce an effective and reproducible electrical coupling between carbon and PEDOT.

3.5. *In vivo assessment of aziridine-EDOT-modified PCMFs (f-CMF 3)*

Finally, the mechanical stability of the PEDOT coating *in vivo*, and the cellular reactions evoked by the microfibers within the neural tissue, are assessed after their chronic implantation for three months within the rat spinal cord. The objective of this experiment is to investigate the effects of the azido-EDOT functionalization on the biological performance of the microfibers, and therefore only washed microfibers are used to avoid confounding results because of non-covalent interactions. Comparisons are performed only regarding the presence or absence of the aziridine-EDOT linker. In both types of microfibers, PEDOT is further coated with a multi-molecular layer of poly-L-lysine, heparin, bFGF, and fibronectin, because this molecular complex substantially improves the integration of PCMFs with neural tissue [8–10].

PCMFs are sufficiently strong to be handled and implanted individually using micro-tweezers, producing negligible damage to the spinal cord during the surgical procedure (Fig. 7a). 1.8-mm long microfibers are introduced from dorsal to ventral in the spinal cord, so that they come into contact with axonal tracts in the white matter and neuronal somas in the grey matter (Fig. 7b). Cutting 60-μm transverse tissue sections reduces damage to the microfibers during the histological processing and allows for the visualization of a large part of the microfiber within a single tissue section, thus facilitating its assessment. After the three-month period, all microfibers could be accurately identified in the site of implantation by transmission light microscopy (Fig. 7e–g). In general, slight tissue impairment is seen because of microfiber implantation, as previously reported for non-washed PCMFs [9]. Nevertheless, azido-EDOT-modified PCMFs are clearly superior to

non-functionalized microfibers regarding the mechanical stability of the conducting polymer coating *in vivo*. When assessed by confocal microscopy (Fig. 7c and d), the control material exhibits substantial PEDOT detachment within the tissue, with numerous polymer fragments remaining in the vicinity of the microfibers (Fig. 7c); whereas the conducting polymer coating is for the most part intact in azido-EDOT modified microfibers (Fig. 7d). About 50 % of the microfiber length shows polymer detachment in controls, compared to 16 % in the functionalized microfibers ($p < 0.001$, Fig. 7i), meaning that azido-EDOT bonding sufficiently strengthens the interphase and is able to counteract traction forces on the polymer exerted by attached cells [60,61]. Importantly, the reduced polymer delamination evokes a weaker reactivity of scarring cells [9] to aziridine-EDOT modified fibers compared to controls (Fig. 7f–h,j), and the functionalized microfibers become fully integrated into the spinal cord in close proximity to neurons (Fig. 7k,l, m).

Preliminary immunohistochemical identification of the reactive cells was performed at one month post-implantation of non-functionalized PCMFs or *f*-PCMFs 3. For this, 10-μm spinal cord sections were stained for cellular markers of microglia and macrophages (IB4, ED1), pericytes and fibroblasts (PDGFRβ), and astrocytes (GFAP) (Fig. S8). In agreement with the reduced PEDOT detachment and cellular reactivity detected with Hoechst and NeuroTrace for *f*-PCMFs 3, little inflammatory and scarring response was evidenced by immunohistochemistry (Fig. S8, right). Moreover, tissue reaction frequently manifested as a tiny (<10 μm) layer of cellular processes contacting the functionalized microfibers, without visible disturbance of the neighbouring tissue. A somewhat larger inflammatory and scarring response apparently occurred around non-functionalized PCMFs (Fig. S8, left).

4. Conclusions

In summary, the clear worsening of the electrochemical performance of *f*-CMFs 1 and *f*-CMFs 2 compared to the starting PCMFs confirms the notion that diazonium salts chemistry disrupts the carbon π-conjugated structure and thus reduce carbon electrical conductivity. Moreover, bonding $EDOT_2$-TPA derivatives at the carbon surface further deteriorates electrical charge transfer when using CMFs and PCMFs for electrical stimulation in liquid electrolytes. On the contrary, [2 + 1] nitrene cycloaddition with azido-EDOT derivatives emerges as a promising method for covalent carbon surface functionalization, preserving the carbon π-network and therefore the conductivity of CMFs. Additionally, it effectively enables PEDOT polymerization, developing a nanostructured CMF surface based on robust covalent bonds, enhancing its resistance to detachment both *in vitro* and *in vivo,* and finally optimizing its integration with neural tissue. This method opens up new possibilities to tailor the electrical and mechanical properties of neuroelectrodes based on CMFs and nanostructured-carbon materials.

CRediT authorship contribution statement

Myriam Barrejón: Writing – original draft, Supervision, Investigation, Conceptualization. **Hugo Vara:** Writing – original draft, Investigation. **Alexandra Alves-Sampaio:** Writing – original draft, Investigation. **Helena Uceta:** Investigation. **Jorge E. Collazos-Castro:** Writing – original draft, Supervision, Conceptualization.

Declaration of competing interest

The authors declare the following financial interests/personal relationships which may be considered as potential competing interests: Myriam Barrejon reports financial support was provided by Junta de Comunidades de Castilla-La Mancha. Jorge Eduardo Collazos-Castro reports financial support was provided by European Innovation Council. Myriam Barrejon reports financial support was provided by Spanish State Agency of Research. J.E. Collazos-Castro and A. Alves-Sampaio share in Spinal Cord Technologies S.L., a spin-off company developing a PCMFs-implant to repair the spinal cord. If there are other authors, they declare that they have no known competing financial interests or personal relationships that could have appeared to influence the work reported in this paper.

Acknowledgements

M.B. acknowledges Junta de Comunidades de Castilla-La Mancha and European Funds (SBPLY/21/180501/000155) for financial support, and the Spanish Government for the Ramon y Cajal contract RYC2021-034815. H.U. thanks MECD for an FPI grant (BES-2017-079649). J.E.C-C. acknowledges the European Innovation Council (EIC) for financial support (DREIMS Transition project, Contract 101136411).

Appendix A. Supplementary data

Supplementary data to this article can be found online at https://doi.org/10.1016/j.carbon.2024.119820.

References

[1] S.L. Barron, S.V. Oldroyd, J. Saez, A. Chernaik, W. Guo, F. McCaughan, D. Bulmer, R.M. Owens, A conformable organic electronic device for monitoring epithelial integrity at the air liquid interface, Adv. Mater. 36 (2024) 2306679, https://doi.org/10.1002/adma.202306679.
[2] Y. Sun, Z. Xiao, B. Chen, Y. Zhao, J. Dai, Advances in material-assisted electromagnetic neural stimulation, Adv. Mater. (2024) 2400346, https://doi.org/10.1002/adma.202400346.
[3] R. Green, M.R. Abidian, Conducting polymers for neural prosthetic and neural interface applications, Adv. Mater. 27 (2015) 7620–7637, https://doi.org/10.1002/adma.201501810.
[4] I. Muguet, A. Maziz, F. Mathieu, L. Mazenq, G. Larrieu, Combining PEDOT:PSS polymer coating with metallic 3D nanowires electrodes to achieve high electrochemical performances for neuronal interfacing applications, Adv. Mater. 35 (2023) 2302472, https://doi.org/10.1002/adma.202302472.
[5] H. Vara, J.E. Collazos-Castro, Biofunctionalized conducting polymer/carbon microfiber electrodes for ultrasensitive neural recordings, ACS Appl. Mater. Interfaces 7 (2015) 27016–27026, https://doi.org/10.1021/acsami.5b09594.
[6] H. Vara, J.E. Collazos-Castro, Enhanced spinal cord microstimulation using conducting polymer-coated carbon microfibers, Acta Biomater. 90 (2019) 71–86, https://doi.org/10.1016/j.actbio.2019.03.037.
[7] S.L. Barron, S.V. Oldroyd, J. Saez, A. Chernaik, W. Guo, F. McCaughan, D. Bulmer, R.M. Owens, A conformable organic electronic device for monitoring epithelial integrity at the air liquid interface, Adv. Mater. 36 (2024) 2306679, https://doi.org/10.1002/adma.202306679.
[8] J.E. Collazos-Castro, C. García-Rama, A. Alves-Sampaio, Glial progenitor cell migration promotes CNS axon growth on functionalized electroconducting microfibers, Acta Biomater. 35 (2016) 42–56, https://doi.org/10.1016/j.actbio.2016.02.023.
[9] A. Alves-Sampaio, C. García-Rama, J.E. Collazos-Castro, Biofunctionalized PEDOT-coated microfibers for the treatment of spinal cord injury, Biomaterials 89 (2016) 98–113, https://doi.org/10.1016/j.biomaterials.2016.02.037.
[10] A. Alves-Sampaio, P. Del-Cerro, J.E. Collazos-Castro, Composite fibrin/carbon microfiber implants for bridging spinal cord injury: a translational approach in pigs, Int. J. Mol. Sci. 24 (2023) 11102, https://doi.org/10.3390/ijms.
[11] H. Vara, G.R. Hernández-Labrado, A. Alves-Sampaio, J.E. Collazos-Castro, Stability of conducting polymer-coated carbon microfibers for long-term electrical stimulation of injured neural tissue, Polymers (Basel) 16 (2024) 2093, https://doi.org/10.3390/polym16142093.
[12] M. Modarresi, A. Mehandzhiyski, M. Fahlman, K. Tybrandt, I. Zozoulenko, Microscopic understanding of the granular structure and the swelling of PEDOT:PSS, Macromolecules 53 (2020) 6267–6278, https://doi.org/10.1021/acs.macromol.0c00877.
[13] C. Boehler, S. Carli, L. Fadiga, T. Stieglitz, M. Asplund, Tutorial: guidelines for standardized performance tests for electrodes intended for neural interfaces and bioelectronics, Nat. Protoc. 15 (2020) 3557–3578, https://doi.org/10.1038/s41596-020-0389-2.
[14] X. Luo, C.L. Weaver, D.D. Zhou, R. Greenberg, X.T. Cui, Highly stable carbon nanotube doped poly(3,4-ethylenedioxythiophene) for chronic neural stimulation, Biomaterials 32 (2011) 5551–5557, https://doi.org/10.1016/j.biomaterials.2011.04.051.
[15] R.A. Green, R.T. Hassarati, L. Bouchinet, C.S. Lee, G.L.M. Cheong, J.F. Yu, C. W. Dodds, G.J. Suaning, L.A. Poole-Warren, N.H. Lovell, Substrate dependent stability of conducting polymer coatings on medical electrodes, Biomaterials 33 (2012) 5875–5886, https://doi.org/10.1016/j.biomaterials.2012.05.017.
[16] T. Boretius, M. Schuettler, T. Stieglitz, On the stability of poly-ethylenedioxythiopene as coating material for active neural implants, Artif. Organs 35 (2011) 245–248, https://doi.org/10.1111/j.1525-1594.2011.01210.x.

[17] L. Ouyang, B. Wei, C.-C. Kuo, S. Pathak, B. Farrell, D.C. Martin, Enhanced PEDOT adhesion on solid substrates with electrografted P(EDOT-NH 2), Sci. Adv. 3 (2017) 1600448. https://www.science.org.

[18] D. Chhin, D. Polcari, C.B.-L. Guen, G. Tomasello, F. Cicoira, S.B. Schougaard, Diazonium-based anchoring of PEDOT on Pt/Ir electrodes via diazonium chemistry, J. Electrochem. Soc. 165 (2018) G3066–G3070, https://doi.org/10.1149/2.0061812jes.

[19] E. Villemin, B. Lemarque, T.T. Vũ, V.Q. Nguyen, G. Trippé-Allard, P. Martin, P. C. Lacaze, J.C. Lacroix, Improved adhesion of poly(3,4-ethylenedioxythiophene) (PEDOT) thin film to solid substrates using electrografted promoters and application to efficient nanoplasmonic devices, Synth. Met. 248 (2019) 45–52, https://doi.org/10.1016/j.synthmet.2018.12.010.

[20] S.F. Cogan, Neural stimulation and recording electrodes, Annu. Rev. Biomed. Eng. 10 (2008) 275–309, https://doi.org/10.1146/annurev.bioeng.10.061807.160518.

[21] X.S. Zheng, Q. Yang, A.L. Vazquez, X. Tracy Cui, Imaging the efficiency of poly(3,4-ethylenedioxythiophene) doped with acid-functionalized carbon nanotube and iridium oxide electrode coatings for microstimulation, Adv. Nanobiomed. Res. 1 (2021), https://doi.org/10.1002/anbr.202000092.

[22] J.D. Benck, B.A. Pinaud, Y. Gorlin, T.F. Jaramillo, Substrate selection for fundamental studies of electrocatalysts and photoelectrodes: inert potential windows in acidic, neutral, and basic electrolyte, PLoS One 9 (2014) e107942, https://doi.org/10.1371/journal.pone.0107942.

[23] R.L. McCreery, Advanced carbon electrode materials for molecular electrochemistry, Chem. Rev. 108 (2008) 2646–2687, https://doi.org/10.1021/cr068076m.

[24] J.D. Randall, D.J. Eyckens, F. Stojcevski, P.S. Francis, E.H. Doeven, A.J. Barlow, A. S. Barrow, C.L. Arnold, J.E. Moses, L.C. Henderson, Modification of carbon fibre surfaces by sulfur-fluoride exchange click chemistry, ChemPhysChem 19 (2018) 3175, https://doi.org/10.1002/cphc.201800997, 3175.

[25] D.J. Eyckens, C.L. Arnold, Ž. Simon, T.R. Gengenbach, J. Pinson, Y. A. Wickramasingha, L.C. Henderson, Covalent sizing surface modification as a route to improved interfacial adhesion in carbon fibre-epoxy composites, Compos. Part A Appl Sci Manuf 140 (2021), https://doi.org/10.1016/j.compositesa.2020.106147.

[26] L. Liu, F. Yan, M. Li, M. Zhang, L. Xiao, L. Shang, Y. Ao, Improving interfacial properties of hierarchical reinforcement carbon fibers modified by graphene oxide with different bonding types, Compos. Part A Appl Sci Manuf 107 (2018) 616–625, https://doi.org/10.1016/j.compositesa.2018.02.009.

[27] M. Jouni, P. Fedorko, C. Celle, D. Djurado, P. Chenevier, J. Faure-Vincent, Conductivity vs functionalization in single-walled carbon nanotube films, SN Appl. Sci. 4 (2022) 132, https://doi.org/10.1007/s42452-022-05016-w.

[28] H. Wilson, S. Ripp, L. Prisbrey, M.A. Brown, T. Sharf, D.J.T. Myles, K.G. Blank, E. D. Minot, Electrical monitoring of sp3 defect formation in individual carbon nanotubes, J. Phys. Chem. C 120 (2016) 1971–1976, https://doi.org/10.1021/acs.jpcc.5b11272.

[29] A. Setaro, M. Adeli, M. Glaeske, D. Przyrembel, T. Bisswanger, G. Gordeev, F. Maschietto, A. Faghani, B. Paulus, M. Weinelt, R. Arenal, R. Haag, S. Reich, Preserving π-conjugation in covalently functionalized carbon nanotubes for optoelectronic applications, Nat. Commun. 8 (2017), https://doi.org/10.1038/ncomms14281.

[30] A. Fiebor, A. Setaro, A.J. Achazi, G. Gordeev, M. Weber, D. Franz, B. Paulus, M. Adeli, S. Reich, Synthesis of multifunctional charge-transfer agents: toward single-walled carbon nanotubes with defined covalent functionality and preserved π system, J. Phys. Chem. C 125 (2021) 19925–19935, https://doi.org/10.1021/acs.jpcc.1c06282.

[31] L. Servinis, L.C. Henderson, T.R. Gengenbach, A.A. Kafi, M.G. Huson, B.L. Fox, Surface functionalization of unsized carbon fiber using nitrenes derived from organic azides, Carbon N Y 54 (2013) 378–388, https://doi.org/10.1016/j.carbon.2012.11.051.

[32] D. Yiłit, S.O. Hacioglu, M. Güllü, L. Toppare, Synthesis and spectroelectrochemical characterization of multi-colored novel poly(3,6-dithienylcarbazole) derivatives containing azobenzene and coumarin chromophore units, Electrochim. Acta 196 (2016) 140–152, https://doi.org/10.1016/j.electacta.2016.02.168.

[33] S. Li, G. Liu, X. Ju, Y. Zhang, J. Zhao, Synthesis, characterization and application of four novel electrochromic materials employing nitrotriphenylamine unit as the acceptor and different thiophene derivatives as the donor, Polymers (Basel) 9 (2017), https://doi.org/10.3390/polym9050173.

[34] F.D. Bellamy, K. Ou, Selective reduction of aromatic nitro compounds with stannous CRLORIDE IN NON acidic and NON aqueous XEDIL'M, Tetrahedron Lett. 25 (1984) 839–842.

[35] G. Trippé-Allard, J.C. Lacroix, Synthesis of nitro- and amino-functionalized π-conjugated oligomers incorporating 3,4-ethylenedioxythiophene (EDOT) units, Tetrahedron 69 (2013) 861–866, https://doi.org/10.1016/j.tet.2012.10.088.

[36] F. Sebest, L. Casarrubios, H.S. Rzepa, A.J.P. White, S. Díez-González, Thermal azide-Alkene cycloaddition reactions: straightforward multi-gram access to Δ2-1,2,3-Triazolines in deep eutectic solvents, Green Chem. 20 (2018) 4023–4035, https://doi.org/10.1039/c8gc01797b.

[37] A. Mahtabani, I. Rytöluoto, R. Anyszka, X. He, E. Saarimäki, K. Lahti, M. Paajanen, W. Dierkes, A. Blume, On the silica surface modification and its effect on charge trapping and transport in PP-based dielectric nanocomposites, ACS Appl. Polym. Mater. 2 (2020) 3148–3160, https://doi.org/10.1021/acsapm.0c00349.

[38] A. Rachini, M. Le Troedec, C. Peyratout, A. Smith, Chemical modification of hemp fibers by silane coupling agents, J. Appl. Polym. Sci. 123 (2012) 601–610, https://doi.org/10.1002/app.34530.

[39] M. Barrejón, R. Rauti, L. Ballerini, M. Prato, Chemically cross-linked carbon nanotube films engineered to control neuronal signaling, ACS Nano 13 (2019) 8879–8889, https://doi.org/10.1021/acsnano.9b02429.

[40] J. Bin Wu, M.L. Lin, X. Cong, H.N. Liu, P.H. Tan, Raman spectroscopy of graphene-based materials and its applications in related devices, Chem. Soc. Rev. 47 (2018) 1822–1873, https://doi.org/10.1039/c6cs00915h.

[41] L. Bokobza, J.-L. Bruneel, M. Couzi, Raman spectra of carbon-based materials (from graphite to carbon black) and of some silicone composites, C (Basel) 1 (2015) 77–94, https://doi.org/10.3390/c1010077.

[42] Z. Li, L. Deng, I.A. Kinloch, R.J. Young, Raman spectroscopy of carbon materials and their composites: graphene, nanotubes and fibres, Prog. Mater. Sci. 135 (2023), https://doi.org/10.1016/j.pmatsci.2023.101089.

[43] R. Samba, Is the enhanced adhesion of PEDOT thin films on electrodes due to sulfur - gold interaction? - an XPS study, Open Surf. Sci. J. 5 (2013) 17–20, https://doi.org/10.2174/1876531901305010017.

[44] T.I.T. Okpalugo, P. Papakonstantinou, H. Murphy, J. McLaughlin, N.M.D. Brown, High resolution XPS characterization of chemical functionalised MWCNTs and SWCNTs, Carbon N Y 43 (2005) 153–161, https://doi.org/10.1016/j.carbon.2004.08.033.

[45] J. Park, M. Yan, Covalent functionalization of graphene with reactive intermediates, Acc. Chem. Res. 46 (2013) 181–189, https://doi.org/10.1021/ar300172h.

[46] A.T. Krasley, E. Li, J.M. Galeana, C. Bulumulla, A.G. Beyene, G.S. Demirer, Carbon nanomaterial fluorescent Probes and their biological applications, Chem. Rev. 124 (2024) 3085–3185, https://doi.org/10.1021/acs.chemrev.3c00581.

[47] P.T.T. Pham, M.M. Bader, Di- and tricyanovinyl-substituted triphenylamines: structural and computational studies, ACS Omega 9 (2024) 11194–11199, https://doi.org/10.1021/acsomega.3c05312.

[48] S. Chen, J. Pei, Z. Pang, W. Wu, X. Yu, C. Zhang, Axial-symmetric conjugated group promoting intramolecular charge transfer performances of triphenylamine sensitizers for dye-sensitized solar cells, Dyes Pigments 174 (2020) 108029, https://doi.org/10.1016/j.dyepig.2019.108029.

[49] J.E. Collazos-Castro, G.R. Hernández-Labrado, J.L. Polo, C. García-Rama, N-Cadherin- and L1-functionalised conducting polymers for synergistic stimulation and guidance of neural cell growth, Biomaterials 34 (2013) 3603–3617, https://doi.org/10.1016/j.biomaterials.2013.01.097.

[50] X. Zhu, X. Han, R. Guo, P. Yuan, L. Dang, Z. Liu, Z. Lei, Vapor-phase polymerization of fibrous PEDOT on carbon fibers film for fast pseudocapacitive energy storage, Appl. Surf. Sci. 597 (2022), https://doi.org/10.1016/j.apsusc.2022.153684.

[51] F. Niu, R. Guo, L. Dang, J. Sun, Q. Li, X. He, Z. Liu, Z. Lei, Coral-like PEDOT nanotube arrays on carbon fibers as high-rate flexible supercapacitor electrodes, ACS Appl. Energy Mater. 3 (2020) 7794–7803, https://doi.org/10.1021/acsaem.0c01202.

[52] W. Zeng, G. Fang, B. Li, Z. Liu, T. Han, J. Wang, F. Liu, P. Fang, X. Zhao, D. Zou, Vibration test method to study elastic stability of porous carbon nanocomposite counter electrode in dye sensitized solar cells, ACS Appl. Mater. Interfaces 5 (2013) 7101–7108, https://doi.org/10.1021/am401422f.

[53] C.L. Arnold, D.J. Eyckens, L. Servinis, M.D. Nave, H. Yin, R.K.W. Marceau, J. Pinson, B. Demir, T.R. Walsh, L.C. Henderson, Simultaneously increasing the hydrophobicity and interfacial adhesion of carbon fibres: a simple pathway to install passive functionality into composites, J. Mater. Chem. A Mater. 7 (2019) 13483–13494, https://doi.org/10.1039/c9ta02436k.

[54] B. Tzaneva, V. Mateev, B. Stefanov, M. Aleksandrova, I. Iliev, Electrochemical investigation of PEDOT:PSS/graphene aging in artificial sweat, Polymers (Basel) 16 (2024), https://doi.org/10.3390/polym16121706.

[55] W.D. Bascom, L.T. Drzal, The Surface Properties of Carbon Fibers and Their Adhesion to Organic Polymers, The contractor report for NASA, 1987.

[56] D.J. Eyckens, J.D. Randall, F. Stojcevski, E. Sarlin, S. Palola, M. Kakkonen, C. Scheffler, L.C. Henderson, Examining interfacial interactions in a range of polymers using poly(ethylene oxide) functionalized carbon fibers, Compos. Part A Appl Sci Manuf 138 (2020), https://doi.org/10.1016/j.compositesa.2020.106053.

[57] C.L. Weitzsacker, M. Xie, L.T. Drzal, Using XPS to investigate fiber/matrix chemical interactions in carbon-fiber-reinforced composites, Surf. Interface Anal. 25 (1997) 53–63, https://doi.org/10.1002/(SICI)1096-9918(199702)25:2<53::AID-SIA222>3.0.CO;2-E.

[58] X. Huang, Fabrication and properties of carbon fibers, Materials 2 (2009) 2369–2403, https://doi.org/10.3390/ma2042369.

[59] Q. Li, A.L. Woodhead, J.S. Church, M. Naebe, On the detection of carbon fibre storage contamination and its effect on the fibre–matrix interface, Sci. Rep. 8 (2018), https://doi.org/10.1038/s41598-018-34609-y.

[60] W. Xie, X. Wei, H. Kang, H. Jiang, Z. Chu, Y. Lin, Y. Hou, Q. Wei, Static and dynamic: evolving biomaterial mechanical properties to control cellular mechanotransduction, Adv. Sci. 10 (2023) 2204594, https://doi.org/10.1002/advs.202204594.

[61] P. Knittel, H. Zhang, C. Kranz, G.G. Wallace, M.J. Higgins, Probing the PEDOT:PSS/cell interface with conductive colloidal probe AFM-SECM, Nanoscale 8 (2016) 4475–4481, https://doi.org/10.1039/c5nr07155k.